Cortical tension overrides geometrical cues to orient microtubules in confined protoplasts

Leia Colin, Antoine Chevallier, Satoru Tsugawa, Florian Gacon, Christophe Godin, Virgile Viasnoff, Timothy Saunders, Olivier Hamant

Cortical tension overrides geometrical cues to orient microtubules in confined protoplasts

Leia Colin[a,1], Antoine Chevallier[a,b,1], Satoru Tsugawa[c], Florian Gacon[a], Christophe Godin[a], Virgile Viasnoff[b,d,e], Timothy E. Saunders[b,d], and Olivier Hamant[a,2]

[a]Laboratoire de Reproduction et Développement des Plantes, Université de Lyon, ENS de Lyon, UCBL, INRAE, CNRS, 69364 Lyon Cedex 07, France; [b]Mechanobiology Institute, National University of Singapore, 117411 Singapore, Singapore; [c]Division of Biological Science, Graduate School of Science and Technology, Nara Institute of Science and Technology, Nara 630-0192, Japan; [d]Department of Biological Sciences, National University of Singapore, 117558 Singapore, Singapore; and [e]Centre National pour la Recherche Scientifique, UMI 3639, 117411 Singapore, Singapore

Edited by Dominique C. Bergmann, Stanford University, Stanford, CA, and approved November 6, 2020 (received for review May 5, 2020)

In plant cells, cortical microtubules (CMTs) generally control morphogenesis by guiding cellulose synthesis. CMT alignment has been proposed to depend on geometrical cues, with microtubules aligning with the cell long axis in silico and in vitro. Yet, CMTs are usually transverse in vivo, i.e., along predicted maximal tension, which is transverse for cylindrical pressurized vessels. Here, we adapted a microwell setup to test these predictions in a single-cell system. We confined protoplasts laterally to impose a curvature ratio and modulated pressurization through osmotic changes. We find that CMTs can be longitudinal or transverse in wallless protoplasts and that the switch in CMT orientation depends on pressurization. In particular, longitudinal CMTs become transverse when cortical tension increases. This explains the dual behavior of CMTs in planta: CMTs become longitudinal when stress levels become low, while stable transverse CMT alignments in tissues result from their autonomous response to tensile stress fluctuations.

microtubule | cell geometry | cortical tension | protoplast | *Arabidopsis*

The relative contribution of cell geometry and forces in cytoskeleton organization has been a long-lasting debate in cell and developmental biology, particularly given the implications for cell division plane determination (1–4). In plants, the organization of the cytoskeleton has a direct impact on cell expansion and morphogenesis (5). Contrary to animal cells, which are often soft and contractile, plant cells are stiff and pressurized. Their mechanics rely on two parameters: turgor pressure (of osmotic origin) and a stiff cell wall which physically constrains the cell (6). Cellulose microfibrils are the main load-bearing components of the wall. Their deposition occurs at the plasma membrane through the activity of cellulose synthases. While the trajectory of cellulose synthase can be biased by preexisting cellulose microfibrils (7), the deposition of new cellulose microfibrils is usually guided by cortical microtubules (CMTs) (8)

In silico simulations of microtubule self-organization suggest that, because of their high persistence length, microtubules should align along the cell long axis (9). Consistently, microtubules growing in confined environments in vitro (microwells) tend to align with the longitudinal axis of the well (10). More recently, wallless plant cells, also called protoplasts, have been confined in agar microwells and hyperosmotic conditions, and CMTs were found to align with the long axis of the protoplast (11). Although such alignments can be observed in nongrowing plant cells in vivo, CMTs are usually transverse in growing cells in vivo (5). To explain this discrepancy, additional factors thus need to be considered.

First, molecular factors at cell edges, like CLASP proteins, could allow CMTs to bend as they grow and, thus, bias the final orientation of the CMT arrays (12). However, microtubules can have transverse and longitudinal orientations in adjacent cells at the shoot apical meristem (13). Furthermore, microtubules can rapidly shift from transverse to longitudinal orientation upon light-induced growth arrest without any change in cell geometry (14). Last, local ablations can induce reorientations of CMTs, without major change in cell geometry (15). Therefore, additional factors must be involved, e.g., to modulate CLASP localization or CMT dynamics. A three-dimensional (3D) computational model managed to recapitulate CMT behavior in the first stages of *Arabidopsis* embryo development by including CLASP-dependent microtubule stability at cell edges and auxin regulation of microtubule dynamics (16).

Although molecular regulators at cell edges are likely to play a key role in CMT orientation, the transverse orientation of CMTs could also be explained without a contribution of cell edges. Indeed, CMTs may indirectly align with maximal tensile stress direction in the cell wall, i.e., the transverse direction for a pressurized elongated cylinder (17, 15). This stress-based scenario is supported by the frequent correlation between predicted tensile stress direction and CMT orientation in several tissues, with or without mechanical perturbations (18). It also provides a mechanism for plant cells to resist tensile stress, as in Wolff's law where bones remodel themselves to resist the load. However, the exact pattern of stress remains debatable, because of the additional complexity brought about by the tissue context. Furthermore, how the CMTs sense the tensile status of the cell wall remains an open problem. In a recent perspective, we proposed that microtubules may be able to autonomously align with changes

Significance

In plants, microtubules largely determine the direction of cell expansion and the orientation of cell division planes. However, what processes orient the microtubules has remained debated. Here, we used microfabricated wells to confine and deform wallless plant cells in a controlled way to analyze the response of microtubules to cell geometry and surface tension. We demonstrate that microtubules align with cell geometry by default, whereas when surface tension increases (e.g. when turgor pressure increases), they align with the direction of maximal tension. Not only does this explain many observations in plant tissues, but it also provides a simple mechanism at the core of plant morphogenesis, in which microtubules can spontaneously align with tension, in a typical self-organized system.

Author contributions: C.G., V.V., T.E.S., and O.H. designed research; L.C., A.C., F.G., and O.H. performed research; L.C., A.C., S.T., F.G., and O.H. analyzed data; and O.H. wrote the paper with assistance from T.E.S..

The authors declare no competing interest.

This article is a PNAS Direct Submission.

[1]L.C. and A.C. contributed equally to this work.

[2]To whom correspondence may be addressed. Email: olivier.hamant@ens-lyon.fr.

This article contains supporting information online at https://www.pnas.org/lookup/suppl/doi:10.1073/pnas.2008895117/-/DCSupplemental.

in maximal tension (18). Here, we adapted a single-cell microwell-based method on wallless *Arabidopsis* protoplast to test this prediction.

Here, we find that CMT orientation depends on curvature anisotropy. CMTs shift their orientation from curvature-derived steric constraints to curvature-derived maximal tension depending on pressurization. Because this behavior does not rely on the presence of a cell wall, this also provides further support for an autonomous microtubule mechanosensing mechanism.

Results

Cortical Microtubules Primarily Align in the Transverse Direction in Confined and Pressurized Protoplasts. CMTs are sensitive to curvature-derived steric constraints due to their high bending stiffness. In elongated cells, they are expected to align longitudinally, i.e., along the direction of lower curvature (or the flattest direction) (Fig. 1*A*). For a pressure vessel, tension and curvature are related by Laplace–Young law, $\Delta P = 2\gamma/R$, with P for pressure, γ for surface tension, and R for radius of the vessel. In short, at equilibrium, maximal tension is in the direction of minimal radius or maximal curvature (*SI Appendix*, *Text* and Fig. S1). In an elongated pressure vessel like a plant cell, maximal tension is transverse to the long axis (Fig. 1*A*). If CMTs are sensitive to curvature-derived tension, they are predicted to align transversely. To test the relative contribution of these opposing curvature-derived cues, we took inspiration from a method initially developed to mimic the cellular microenvironment for animal cells (19). To be able to rapidly deform the cell cortex and obtain simple global geometries, we used wallless plant cells (spherical protoplasts) and confined them in rectangular wells. We then modified their pressurization using solutions of different osmolarity (Fig. 1*B*; see *Materials and Methods*; *SI Appendix*, Fig. S2*A*). Note that there was no detectable wall synthesis within the timeframe of the experiment (*SI Appendix*, Fig. S3).

To confirm the shape and pressurized status of protoplasts, we monitored protoplast deformation, using the *pUbQ10::LTI6b-TdTomato* membrane marker reporter line (Fig. 1 *C–F*). When viewed from the bottom, confined protoplasts appeared elongated in rectangular wells. Orthogonal sections and 3D reconstruction confirmed their pressurized status, with hemispherical top and bottom membranes (Fig. 1 *C–F* and Movies S1 and S2). The protoplasts only appeared to be geometrically deformed laterally, as if they were confined between two plates. Importantly, such confinement did not induce sharp edges, as the protoplast contour remained almost tangential to the microwell walls (Fig. 1 *C–F* and *SI Appendix*, Fig. S2*B*). Thus, the cell-edge contribution to CMT behavior is not explicitly studied in this work. Using the measured aspect-ratio (length/width between 1.13 and 1.17), we confirmed that predicted maximal tensile stress is transverse in confined protoplasts (Fig. 1*G* and *SI Appendix*, *Text*).

To follow microtubule dynamics, we used the microtubule reporter line *p35S::GFP-MBD* (Fig. 1*H*) (Microtubule Binding Domain of rat MAP4; ref. 15). Note that protoplasts were still alive after 17 h in the wells, confirming that this environment is not toxic for the protoplast, as already shown for animal cells (Fig. 1*I*). To test whether CMTs exhibit a bias in their orientation in these conditions, we used 15 × 20 μm microwells, and we observed the GFP-MBD signal 2 h after transfer from 600 mOsmol/L to 280 mOsmol/L mannitol. Qualitatively, we observed a wide diversity of CMT behaviors in confined and pressurized protoplasts (Fig. 1*J*). To quantify this pattern, we measured the orientation of microtubules on small regions of interest (ROIs), thus providing a local quantification of each microtubule segment, using the subcellular fibrillar tool (SFT hereafter, Fig. 1*K*; ref. 20). Typically, we obtained a distribution of orientations per protoplast. This method revealed that CMTs in confined and pressurized protoplasts indeed exhibit a bias in the transverse orientation (n = 126 protoplasts, $P < 10^{-3}$ [Rayleigh's test for uniformity], Fig. 1*L*). This conclusion was independent on the analysis method, as a similar trend was obtained using the ImageJ plugin OrientationJ (*SI Appendix*, Fig. S4).

We also checked whether local curvature could affect the CMT orientation globally. To do so, we analyzed a subset of confined protoplasts that were large enough to touch four walls of the wells, instead of just two, when confined (*SI Appendix*, Fig. S2*C*). Our analysis revealed the same transverse bias in CMT orientation in this population of protoplasts, consistent with a response of CMTs to global curvature anisotropy in our setup (*SI Appendix*, Fig. S2*D*). Altogether, this suggests that CMTs can align with maximal tension. This also suggests that such alignment does not depend on the cell wall.

Challenging the Transverse Orientation of CMTs in Confined and Pressurized Protoplasts. To challenge our finding, we performed three additional tests. First, in principle, the transverse bias could be caused by the adhesion of the protoplast to the well edges. Yet, the tangential curvature suggests very weak adhesion to the well sides (Fig. 1*D* and *SI Appendix*, Fig. S2*B*). To check this formally, we pretreated the microwells with pluronic acid, which is classically used in cell cultures to inhibit surface-tissue adhesion (21). In these conditions, we still observed a transverse bias in CMT orientation (n = 29 protoplasts, $P < 10^{-3}$ [Rayleigh's test for uniformity], Fig. 2 *A* and *B*).

Second, if the bias in orientation truly depends on curvature anisotropy, it should be lost in square-shaped wells. To test this, we used 14 × 14 μm microwells. In these wells, as expected, we did not observe any significant bias in CMT orientation (n = 74 protoplasts, P = 0.11 [Rayleigh's test for uniformity], Fig. 2 *C* and *D*).

Last, if CMTs align with the direction of maximal tension at the protoplast cortex, they should do so for any rectangular geometry, with the bias increasing when curvature anisotropy increases, in accordance with the Laplace–Young law. To test that prediction, we used 12 × 40 μm microwells. As expected, we found a significant bias of CMT orientation in the transverse direction (n = 99 protoplasts, $P < 10^{-3}$ [Rayleigh's test for uniformity], Fig. 2 *E* and *F*). Interestingly, the bias in the transverse direction was indeed stronger in the 12 × 40 μm microwells than in the 15 × 20 μm microwells ($P < 10^{-3}$, null hypothesis: mean angle of 12 × 40 > mean angle of 15 × 20) permutation test). Altogether, this supports a scenario in which CMTs orient with predicted maximal tension in confined and pressurized protoplasts.

Pressurization Determines CMT Orientation in Confined Microwells. If CMTs align with the pattern of tension for a given geometry, this alignment should become less pronounced when tension decreases. Recently, the analysis of protoplasts confined in agar wells in hyperosmotic conditions has shown that CMTs align with the long axis of the protoplast, consistent with this prediction (11). To test this in our setup, protoplasts were introduced in 12 × 40 μm microwells in a hypertonic solution (600 mOsmol/L mannitol) as previously, and then the protoplasts were exposed to an even more hypertonic solution (800 mOsmol/L mannitol, compared with 280 mOsmol/L mannitol). As expected, because of reduced pressurization, protoplasts were more deformable (Fig. 3*A* and *SI Appendix*, Fig. S4). In these conditions, the transverse CMT bias was lost in all replicates 2 h after the addition of the hypertonic solution. Instead, a global bias in the longitudinal distribution was observed (n = 97 protoplasts, $P < 10^{-3}$ [Rayleigh's test for uniformity], Fig. 3 *B* and *C*).

Consistent with their reduced pressure-dependent stiffness and increased deformability, several protoplasts exhibited a very elongated shape (Fig. 3*B*). This increased range of shapes allowed us to check the correlation between protoplast aspect-ratio and CMT orientation. We first calculated a mean CMT orientation per protoplast, with the OrientationJ, Dominant Direction plugin, and second, we calculated a deformation ratio (*Materials and Methods*). We found that average CMT orientation is longitudinal

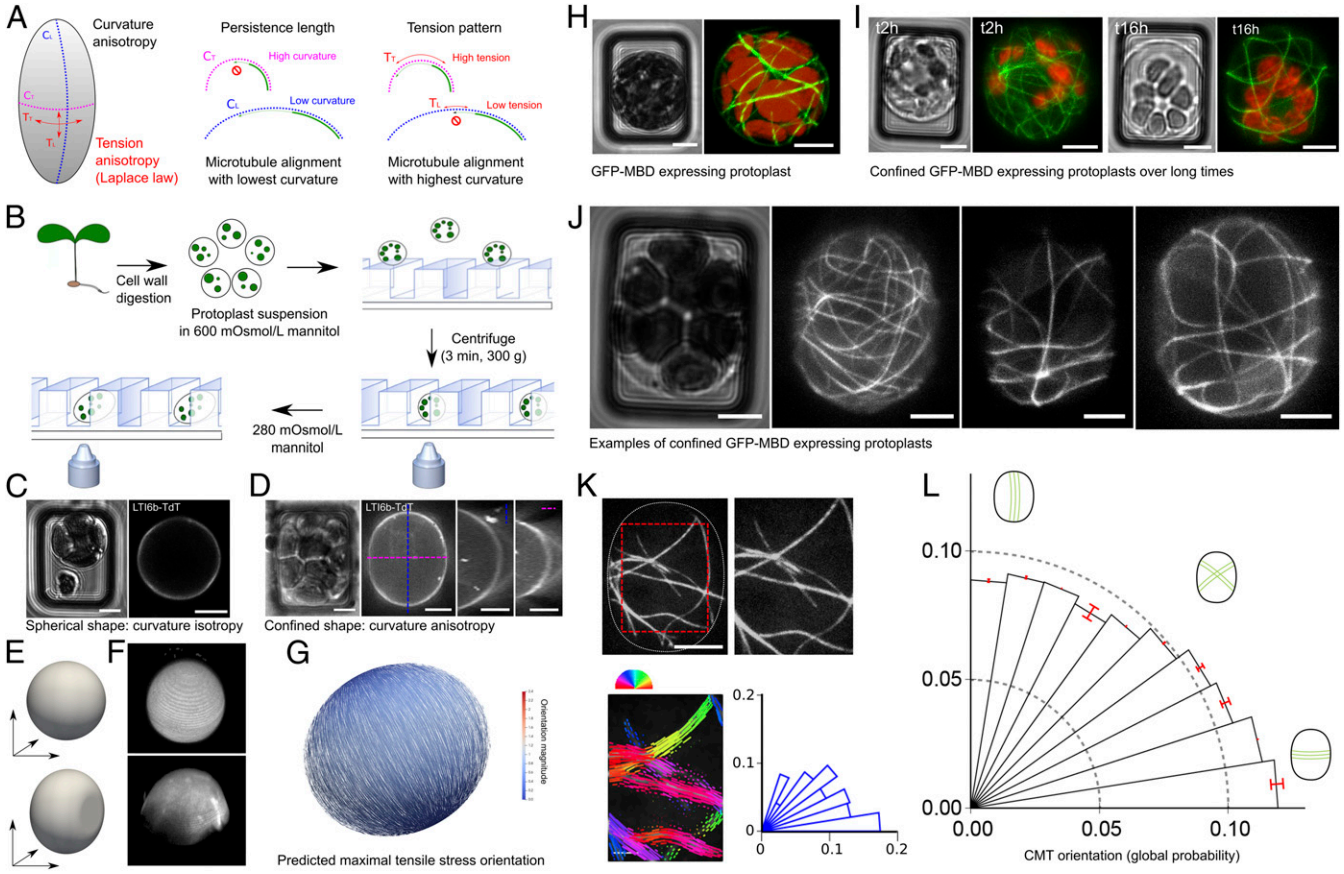

Fig. 1. Cortical microtubule response to protoplast confinement. (*A*) Main hypothesis: In a confined protoplast, transverse curvature is higher than longitudinal curvature, resulting in a competition between steric and mechanical cues; lower curvature would accommodate microtubule high bending stiffness, while high curvature would prescribe high tension to which microtubules may align with. (*B*) Schematic summary of the protocol used to confine and image protoplasts in microwells. (*C*) *pUbQ10::LTI6b-TdTomato* (membrane marker) protoplast. Transmitted light channel (*Left*) and TdTomato fluorescence channel (*Right*). (*D*) *pUBQ10::LTI6b-tdTomato* images of a deformed and turgid (280 mOsmol/L mannitol) protoplast. Transmitted light channel (*Left*) and fluorescence of TdTomato channel (*Right*). Orthogonal views are presented at *Right*. (*E*) FEM representation of an unconfined protoplast (sphere, *Upper*) and confined protoplast (*Lower*). (*F*) Three-dimensional reconstruction from confocal stacks for an unconfined (*Upper*) and confined (*Lower*) protoplast expressing *pUBQ10::LTI6b-tdTomato* (280 mOsmol/L mannitol). (*G*) FEM simulation for a confined ellipsoid with an aspect-ratio (length/width) of 1.15, as measured in our experiments (1.13–1.17). Maximal tensile stress is predicted to be transverse, following Laplace–Young law. (*H*) *p35S::GFP-MBD* protoplast. (*Left*) Transmitted light channel. (*Right*) GFP fluorescence channel. Red, autofluorescence of chloroplasts; green, microtubule signal. (*I*, *Left*) Transmitted light channel and GFP fluorescence channel, 2 h after protoplast's insertion in the microwell. (*I*, *Right*) Transmitted light channel and GFP fluorescence channel, 16 h after protoplast's insertion in the microwell. Two different protoplasts are shown. (*J*) Examples of *p35S::GFP-MBD* protoplast images, illustrating the diversity of microtubule orientations in 15 × 20 μm microwells in pressurized (280 mOsmol/L mannitol) and confined protoplasts. Protoplasts were imaged 2 h after their transfer into hypotonic solution. (*K*) Analysis of CMT orientation with SFT. The cropped zone is delineated with the dotted red lines. The orientation of CMTs in each ROI is color coded. Polar histograms represent the CMT angle distribution for the protoplast. Each bar corresponds to an angle range of 9°. (*L*) Polar histograms of the probability of CMT orientations (classes of 9° angles) in all protoplasts, confined in 15 × 20 μm microwells, imaged 2 h after their transfer in 280 mOsmol/L mannitol (n = 126 protoplasts, three independent replicates). (Scale bars, 5 μm.)

for the most elongated protoplasts (Fig. 3 *D* and *F*). Yet, such a bias was significantly reduced in protoplasts with an aspect-ratio below 2.5; in such protoplasts, CMT orientation was more isotropic ($p_{<2.5}$ = 0.052 vs. $p_{>2.5}$ = 0.020 [Rayleigh's test for uniformity], Fig. 3 *D* and *E*). Altogether, this confirms that the transverse orientation of CMTs depends on the degree of protoplast pressurization. Our results also suggest that CMTs align with geometry when surface tension is low, i.e., the long axis of the protoplasts.

Microtubule Orientation Respond to Deviations in Cortical Tension. So far, our results are consistent with CMTs aligning with predicted maximal tension at the protoplast cortex. Results obtained in vitro suggest that the microtubule response to tension is transient (22). Taking advantage of time-lapse imaging within our setup, we next investigated the transient nature of the microtubule response in vivo.

When observing a confined protoplast over a long time, changes in CMT orientations could be detected, further confirming that the protoplast is alive. Note that CMT reorientations appeared slow when compared to in vivo data. In the example shown in *SI Appendix*, Fig. S5 *A* and *B*, subtle changes were observed (see also Movie S3): Upon transfer from 800 mOsomol/L to 400 mOsmol/L, the initial bias in the longitudinal orientation was progressively lost in favor of a more uniform, and even transverse, orientation and then back to longitudinal. As shown in *SI Appendix*, Fig. S5 *C–E*, CMTs could completely change their orientations while being confined over long time periods. Within the same geometry, protoplasts can thus acquire new CMT orientation depending on pressure.

The use of 800 mOsm/L mannitol conditions can generate highly deformed protoplasts and is perfectly adapted to show the contribution of cell geometry, as an aspect-ratio superior to 2.5

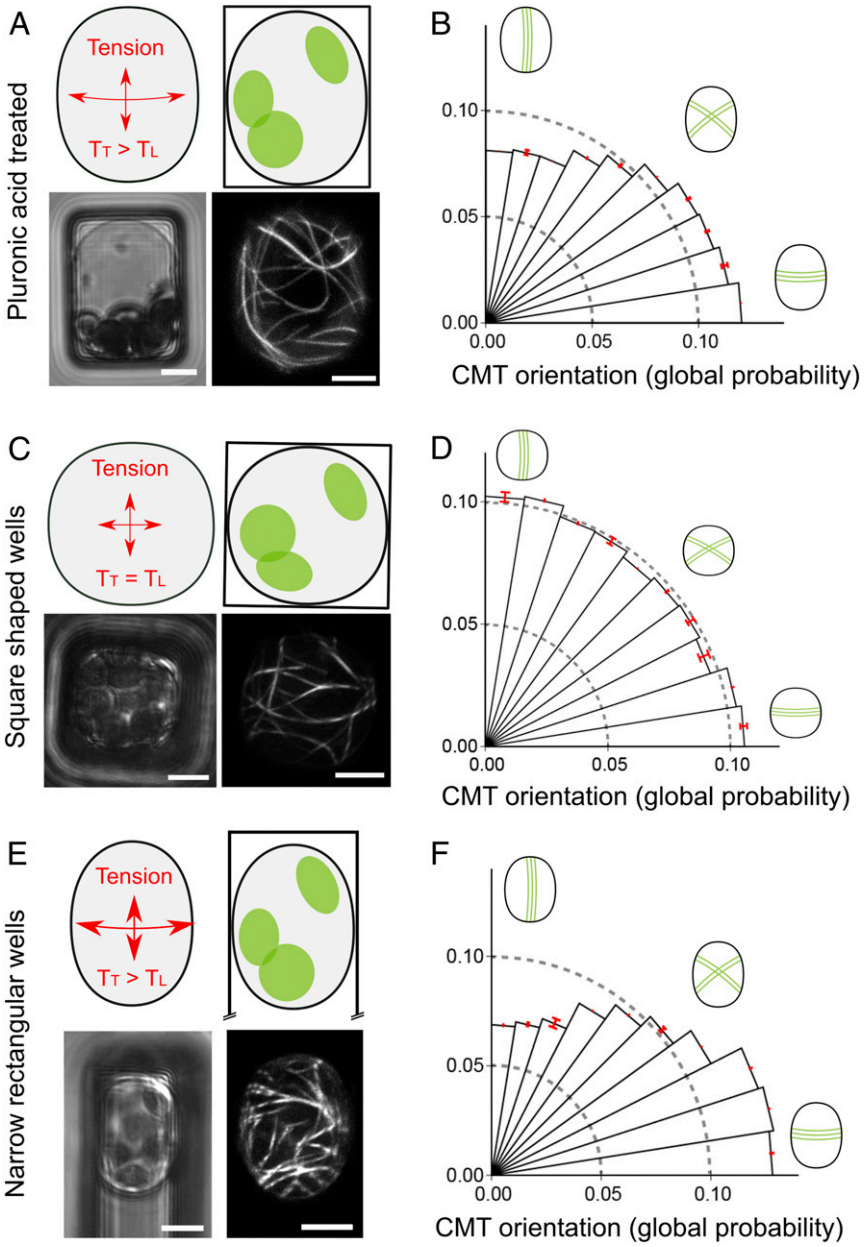

Fig. 2. Challenging the transverse orientation of CMTs in confined and pressurized protoplasts. (*A*) Schematic representation of the stress pattern in 15 × 20 μm microwell. *p35S::GFP-MBD* pressurized protoplast, confined in 15 × 20 μm microwell, was pretreated with pluronic acid to reduce protoplasts adhesion to the well sides, and in 280 mOsmol/L mannitol. (*Lower Left*)Transmitted light channel. (*Lower Right*) GFP fluorescence channel. (*B*) Polar histograms representing the probability of CMT orientations (classes of 9° angles) in protoplasts confined in 15 × 20 μm passivated microwells and imaged 2 h after their transfer to 280 mOsmol/L mannitol ($n = 29$ protoplasts). (*C*) Schematic representation of protoplast curvature in 14 × 14 μm square-shaped wells. *p35S::GFP-MBD* protoplast was confined in 14 × 14 μm microwell in 280 mOsmol/L mannitol. (*Lower Left*)Transmitted light channel. (*Lower Right*) GFP fluorescence channel. (*D*) Polar histograms representing the probability of CMT orientations (classes of 9° angles) in protoplasts confined in 14 × 14 μm microwells and imaged 2 h after their transfer to 280 mOsmol/L mannitol ($n = 74$ protoplasts, three independent replicates). (*E*) Schematic representation of protoplast curvature in 12 × 40 μm wells. *p35S::GFP-MBD* protoplast was confined in 12 × 40 μm microwell in 280 mOsmol/L mannitol. (*Lower Left*) Transmitted light channel. (*Lower Right*) GFP fluorescence channel. (*F*) Polar histograms representing the probability of CMT orientations (classes of 9° angles) in protoplasts confined in 12 × 40 μm microwells, imaged 2 h after their transfer to 280 mOsmol/L mannitol ($n = 99$ protoplasts, four independent replicates). (Scale bars, 5 μm.)

was required to induce a significant bias in CMT orientation along the long axis of the protoplast (*SI Appendix*, Fig. 3 *D* and *E*, and ref. 11). However, such high osmolarity may also induce artifacts, or even trigger slowed life mechanisms, as in dormant seeds for instance (23). In fact, high osmolarity has been proposed to slow microtubule dynamics in yeast because of cytoplasmic crowding (24). We thus focused on the comparison between 600 and 280 mOsm/L mannitol, even if, in these conditions, we could not induce such high aspect-ratios. Long-term kinetics showed changes in CMT orientation during the switch from hyperosmotic to hypoosmotic conditions and vice versa (*SI Appendix*, Figs. S6–S8 and Movies S4–S6). CMT arrays appear to retain their ability to modify orientation when osmotic conditions fluctuate. Strikingly, as we followed CMT behavior in protoplasts being transferred from 600 to 280 mOsmol/L mannitol, we observed new microtubules appearing in the transverse

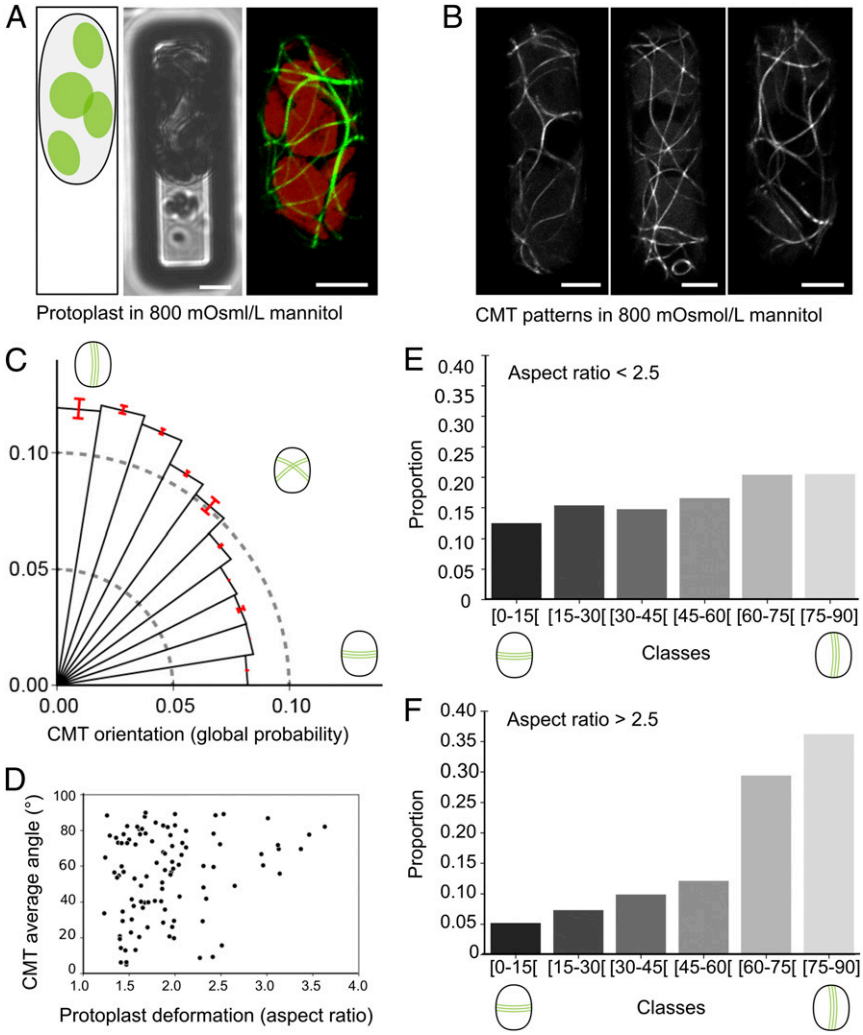

Fig. 3. Pressurization determines CMT orientation in confined microwells. (*A*) *p35S::GFP-MBD*–confined protoplast in 12 × 40 μm microwell in hypertonic solution (800 mOsmol/L mannitol). (*Left*) Schematic representation. (*Center*) Transmitted light channel. (*Right*) GFP fluorescence channel. (*B*) Examples of highly deformed *p35S::GFP-MBD* protoplasts in 800 mOsmol/L mannitol. (*C*) Polar histograms representing the probability of CMT orientations (classes of 9° angles) in protoplasts in hypertonic solution and imaged 2 h after their transfer to 800 mOsmol/L mannitol ($n = 102$ protoplasts, six independent replicates). (*D*) Scatterplot representing the dominant orientation of CMTs in each protoplast (OrientationJ, Dominant direction plugin analysis) according to the protoplast aspect-ratio after confinement (each dot represents a protoplast, $n = 97$ protoplasts, six independent replicates). (*E* and *F*) CMT orientations (classes of 15° angles) for protoplasts with an aspect ratio inferior to 2.5 ($n = 90$ protoplasts) (*E*) and superior to 2.5 ($n = 12$ protoplasts) (*F*). (Scale bars, 5 μm.)

orientation (Fig. 4*A*, arrows; *SI Appendix*, Figs. S6 and S8, arrows). This is consistent with a scenario in which transverse tension promotes the polymerization of microtubules in that direction.

To test whether CMTs are able to maintain their stress-derived transverse orientation in the long term, without any imposed change in osmolarity, we examined CMT orientations in protoplasts 16 h after the transfer from 600 to 280 mOsmol/L mannitol (Fig. 4*B*). In such conditions, protoplast shape appeared stable. It is possible that many aspects of the protoplast change in this timeframe (e.g., plasma membrane composition, metabolism), yet transverse curvature remains higher than longitudinal curvature. After 16 h, the transverse CMT bias was lost in 12 × 40 μm microwells ($n = 69$ protoplasts, $P < 10^{-3}$ (null hypothesis: mean angle in 12 × 40 μm microwells at 16 h < mean angle in 12 × 40 μm microwells at 2 h), Fig. 4 *C* and *D*). This is consistent with a scenario in which CMTs align with changes in maximal tension and usually return to their geometry-derived orientation if no more changes in tension direction occur.

Discussion

We have demonstrated that CMTs can change their orientation in confined protoplasts without cell walls or sharp edges. This provides a hierarchical scenario: 1) CMTs align with the long axis of the cell by default, because of their high flexural rigidity (also consistent with refs. 9 and 11); 2) tension promotes alignment of CMTs with maximal tension, which is transverse for an elongated cell; and 3) although cell edges are dispensable for CMT self-organization and reorientation, the associated molecular regulators can modulate the final CMT orientation in vivo.

The microtubule response to mechanical stress is supported by many studies from different groups, on different plant parts, and in response to different mechanical perturbations (17, 25, 15, 26). Yet, most of the obtained results so far relate to CMT behavior in tissues, in which the exact stress pattern can be difficult to predict. Here, using a confined protoplast protocol, we not only demonstrate that a full cell wall is not required for the microtubule response to stress, but we also show that microtubules are able to

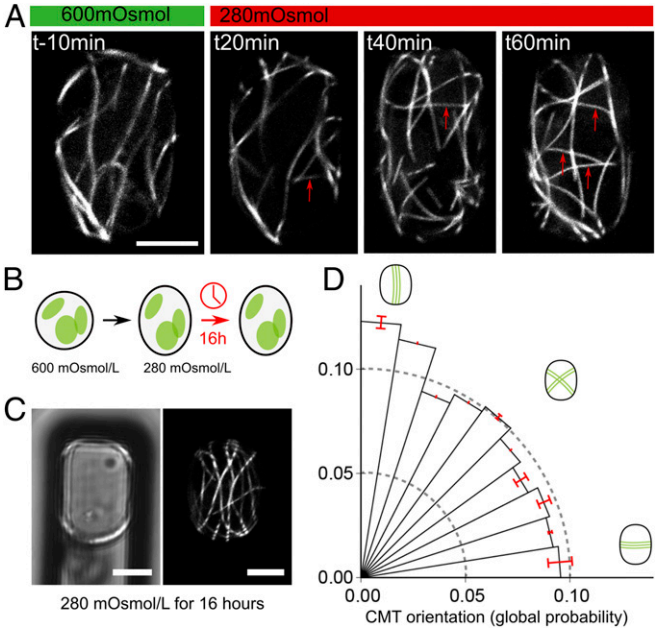

Fig. 4. Pressurization determines CMT orientation in confined microwells. (*A*) Time-lapse imaging of a *p35S::GFP-MBD*–confined protoplast in a 12 × 40 μm microwell as it is transferred from 600 to 280 mOsmol/L mannitol (at t = 0 min). New transverse CMTs progressively appear upon pressurization (red arrows). (*B*) Schematic representation of the experiment: Protoplasts were isolated in 600 mOsmol/L mannitol and then confined 12 × 40 μm microwells in the presence of 280 mOsmol/L mannitol for 16 h. (*C*) *p35S::GFP-MBD*–confined protoplast in a 12 × 40 μm microwell, imaged 16 h after transfer to 280 mOsmol/L mannitol. (*Left*) Transmitted light channel. (*Right*) GFP fluorescence channel. (*D*) Polar histograms representing the probability of CMT orientations (classes of 9° angles) in protoplasts in 12 × 40 μm microwells and imaged 16 h after transfer to 280 mOsmol/L mannitol (n = 72 protoplasts, three independent replicates). (Scale bars, 5 μm.)

perceive both cell geometry and cortical tension, depending on a threshold in cortical tension. These results are consistent with the proposal that microtubules may spontaneously orient with maximal tension (18), building on in vitro data on stretched microtubules (27) and on the predicted weakness of the geometrical cue for CMT self-organization (9).

Here, we have focused on the role of cell geometry and cortical tension in determining CMT behavior. Yet, cell edges are also important players to explain CMT orientations in vivo (12, 16). Interestingly, the three contributions—cell geometry, cortical tension, cell edges—are highly interconnected. In particular, curvature depends on cell geometry, prescribes tension stress pattern, and can locally become an obstacle for CMTs at cell edges. One avenue for future studies will be to check whether cell edge components are sensitive to shape or tension and, in turn, whether changes in tension can modify global shape and cell edge geometry. At this stage, we also cannot completely exclude the possibility that specific regulators may be recruited at cell edges, independent from cell geometry and tension.

The MBD construct induces known artifacts, such as extra microtubule bundling and twisted organs (28). One cause of our observed transverse CMT bias in pressurized protoplasts may be the MBD domain. However, longitudinal CMTs were observed in protoplasts confined in agar wells using the same GFP-MBD line (29). Furthermore, as protoplast curvature and aspect-ratio do not change over 16 h, and CMT orientation can change, the MBD domain does not prevent CMT reorientation, independent of curvature or protoplast geometry.

More interestingly, our results support a scenario in which CMTs respond to changes in tension, rather than the pattern of tension at steady state. This observation is consistent with in vitro data on transiently stretched microtubule networks (22). This allows us to revisit the role of cell geometry in defining microtubule orientation. As our system imposes a stable geometry, it allows us to reveal that the microtubule response to stress requires fluctuations in shape and stress pattern (cycles of pressurization and depressurization in our experiments). Fluctuations are often viewed as extra noise on top of an average situation. Here, we provide clear evidence that, instead, fluctuations allow cells to perceive stress, to which they respond. In other words, the average orientation of microtubules in cells seem to be the result of stress fluctuation rather than a product of cell geometry alone.

Is there evidence of such stress fluctuations in planta? Low frequency fluctuations could easily be explained by circadian turgor rhythms. Nastic movement of leaves and stems further suggest that variations in the mechanical status of the plant are subcircadian (30). The analysis of hypocotyl growth also suggests that shorter period fluctuations exist in *Arabidopsis* seedlings, from which our protoplasts were extracted (31). Last, the calcium waves at the shoot apical meristem, every 10–30 min, may indicate that mechanical fluctuations in plant tissues are underestimated (32). These different systems suggest that such fluctuations may be the norm, rather than the exception.

Our setup opens avenues for other future research questions. In particular, such a single cell system offers the opportunity to revisit the molecular factors involved in the microtubule—cell wall continuum, which remains largely ill-described. This may also prove useful for the analysis of other cortical factors like auxin transporters. Our protocol may fill a missing link in the study of plant mechanotransduction, playing a similar role as in vitro studies of fibroblasts in animal mechanotransduction studies, i.e., to provide a context in which mechanical parameters are better controlled and in which conclusions can then be tested in a multicellular context.

Materials and Methods

Experiments were conducted in two laboratories (Mechanobiology Institute [MBI] in Singapore and Laboratoire de Reproduction et Développement des Plantes [RDP] in Lyon, France).

Plant Growth Conditions (MBI and RDP). At MBI, *Arabidopsis thaliana* plants were grown at room temperature in long-day conditions (16 h/8 h light/dark cycle), on medium containing 11.94 g/L of *Arabidopsis* medium (Duchefa) supplemented with 2 mM $Ca(NO_3)_2$, pH 5.8 for 7–15 d. At RDP, *A. thaliana* seeds were sown on MS (Murashige and Skoog) medium and grown in vitro in long-day conditions (16 h/8 h light/dark period) for 7–15 d. The microtubule reporter line (*p35S::GFP-MBD*) and the plasma membrane reporter line (*pUbq10::LTI6b-TdTomato*) were previously described (15).

Protoplast Generation (MBI and RDP). Protoplasts were obtained from 7- to 15-d-old seedlings. Cell wall was digested through seedling immersion in 1.1 mL of solution A (D-Mannitol [600 mOsmol/L], $CaCl_2$ [2 mM], $MgCl_2$ [2 mM], L-ascorbic acid [1 mM], BSA [3.5 mg/mL], MES [10 mM at pH 5.5]) supplemented with wall digesting enzymes (Cellulysine [Calbiochem] [17 mg/mL], Cellulase RS [17 mg/mL], Pectolyase Y23 [0.4 mg/mL]). Ca. 10 seedlings were incubated in the enzymatic solution. At RDP, the incubation lasted for 2 h under slow agitation on a rotating wheel (12 rpm) at room temperature (i.e., ca. 21–25 °C). At MBI, the incubation lasted overnight under agitation (40 rpm) at room temperature (i.e., ca. 20 °C). After incubation, the seedling suspension was aspired up and down five or six times using a 1-mL pipette to break the tissue and free the protoplasts. Samples were centrifuged at 1,000 rpm for 4 min, the supernatant was discarded and protoplasts were washed for 1 min with 1 mL of solution A. A second centrifugation (1,000 rpm, 4 min) was performed, and most of the supernatant was discarded, keeping ca. 200 μL of a suspension of protoplasts in solution A. Protoplasts were then placed at 4 °C for 30 min. We did not select for a specific type of protoplasts (e.g., with different size or different number of chloroplasts, *SI Appendix*, Fig. S2*A*) to ensure that our observations were robust with respect to the diversity of protoplasts. The digestion of the cell wall was

confirmed by the absence of calcofluor (cellulose dye) and propidium iodide (pectin dye) staining (*SI Appendix*, Fig. S3).

Microwell Fabrication (MBI). A PDMS (90% silicone elastomer base, Sylgard + 10% silicone elastomer curing agent, Sylgard) stamp was first fabricated using lithography (SU8 method) and silanized (Trichloro(1H,1H,2H,2H-perfluorooctyl)-silane, Aldrich) for 2 h under vacuum. PDMS was then poured on the mold and degassed 15 min at 10 mBar before curing 2 h at 80 °C. After removing, the stamp was cut into pieces of about 1 cm × 0.5 cm and silanized 2 h under vacuum. Microwells were obtained by pressing PDMS molds into a drop of ultraviolet (UV) curable monomers of Norland Optical Adhesive 73 (NOA73), beforehand deposited in ibidi dish (ibidi glass bottom dish 35 mm). At MBI, UV curing was performed with UV-KUB 9 (Kloé SA, 200 mW/cm^2) for 30 s. At RDP, UV curing was performed with UV-KUB 2 (Kloé SA, 40 mW/cm^2) for 3 min. Ibidi dish were filled with 3 mL of water, and the PDMS mold was carefully removed with tweezers to avoid formation of air bubbles in the microwells. For a more detailed protocol, see ref. 19.

Surface Passivation with Pluronic Acid. To test the contribution of protoplast adhesion to CMT behavior, microwells were treated for 30 min at 37 °C with 2% (vol/vol) pluronic acid (a nonionic surfactant). The negative impact of pluronic acid on protoplast adhesion was confirmed with the following control experiment: We added 300 μL from the same protoplast's suspension on Ibidi dish either pretreated for 30 min at 37 °C with 2% (vol/vol) pluronic acid or incubated with water in the same conditions. Protoplasts were let to sediment for 2 h. Then, the Ibidis were tilted in a similar way (being attached to the same support) to let the protoplast suspension flow down and the number of remaining protoplasts (i.e., still attached to the Ibid's coverslip) was counted. Many protoplasts were still attached in the control (water) Ibidi (n = 6,216 protoplasts), whereas, in the pluronic-treated Ibidi, fewer protoplasts were present (n = 2,003 protoplasts) and most of them were located at the coverslip-plastic edge of the Ibidi. This confirms that the pluronic acid surfactant hinders adhesion of *Arabidopsis* protoplasts.

Protoplast Confinement (MBI and RDP). Microwells in Ibidi dishes were washed with solution A before protoplast confinement. After removing solution A from the Ibidi dish, 50 μL of protoplast solution was deposited on microwells and let to sediment at room temperature for 5 min. The Ibidi dish was then centrifuged at 300 × g for 3 min (using a plate holder). The step of sedimentation increases the number of confined protoplasts into the microwells. After centrifugation, 3 mL of solution B (identical to solution A except for D-Mannitol [280 m to 800 mOsmol/L]) were added to induce hypoosmotic (D-Mannitol 280 mOsmol/L), mild hypoosmotic (D-Mannitol 400 mOsmol/L) or hyperosmotic (D-Mannitol 800 mOsmol/L) shock.

Microscopy and Imaging (MBI and RDP). For the experiments reported in Figs. 1–3, live imaging started 2 h after the addition of the hypotonic or hypertonic solution and stopped ∼2 h later. For the experiments reported in Fig. 4, kinetics was performed immediately after the addition of solution B, and late time points (t = 16 h) were also considered.

At MBI, images were acquired on a spinning-disk confocal microscope (Yokogawa W1 on Nikon T1E) and an inverted confocal LSM710 microscope (Zeiss) using 100× lens (oil immersion, N.A.= 1.45 [Nikon] and 1.46 [Zeiss]). At RDP, images were acquired on LSM800 inverted confocal microscope (Zeiss) using 63x lens (oil immersion, N.A. = 1.4).

Time-lapse experiments: Protoplasts were prepared as described above and were confined in 12 × 40μm microwells in hypertonic solution (Movie S1: 800 mOsmol/L mannitol, and Movies S2–S4: 600 mOsmol/L mannitol). The Ibidi dishes were installed under the microscope, and specific microwell positions on plate were recorded. Movie S3 was performed on widefield inverted microscope (Zeiss) using 63× lens (oil immersion, N.A. = 1.4) and Movies S1, S2, and S4–S6 were performed on LSM800 inverted confocal (Zeiss), using 63× lens (oil immersion, N.A. = 1.4). For Movie S3, the 800 mOsmol/L mannitol solution was replaced by a 400 mOsmol/L mannitol solution, and imaging started immediately after the addition of the 400 mOsmol/L mannitol solution. Images were taken every 30 min for 8 h. For Movies S4–S6, imaging started in 600 mOsmol mannitol solution, and at t = 0, the 600 mOsm/L mannitol solution was replaced by the 280 mOsm/L mannitol solution. Further changes in solutions were performed every 2 h, as shown in the figures. Images were taken every 20 min until protoplast's death.

Cell wall staining: *p35S::GFP-MBD* seedlings (positive control for the dyes) and *p35S::GFP-MBD* protoplasts (obtained after 2 h of enzymatic digestion at RDP) were immersed in solution A containing either 0.3 mg/mL of propidium iodide, which stains demethyl-esterified pectins (33), for 10 min or 0.01% of calcofluor, which stains cellulose microfibrils (34), for 15 min. Seedlings and protoplasts were then imaged on LSM800 inverted confocal microscope as described above. The absence of cell wall was tested immediately after digestion and 22 h after digestion.

Image Processing. The first five slices of the confocal stack were used to make a maximal projection. This removed most of the cytoplasmic signal in the images, including cytoplasmic microtubules. Then, all projections corresponding to one technical replicate were assembled as a stack, projections were aligned with the ImageJ plugin AlignSlice, and all images were cropped to keep the central part of the protoplast (to avoid artifacts on the sides of the cells due to the projection). Finally, a Gaussian blur (radius: 2.00 pixels) was performed on the images. Then, microtubule orientation analysis was performed using SFT (20). This method is based on nematic tensors and provide orientation and anisotropy of the microtubule arrays. Each protoplast is divided in ROIs, and the orientation of each ROI is then analyzed. On average, this represented 394 ROIs (i.e., CMT fragment angles) per protoplast. The orientation is measured from an imaginary horizontal line, and the angle between this line and the ROIs is calculated. A polar histogram was constructed, displaying the global probability for each orientation to belong to a class of angle, ranging from 0° to 90°. Thus, 10 classes of angles of 9° were formed, from 0°–9° to 81°–90°. We used the probability density function where (probability) = sum of (probability density function) × (bin width) over bins. When 10 classes of angles (0–90°) are defined, bin width is (π/2)/10 ∼ 0.157. In the figures, we plotted the probability in each bin, which is (probability density function) × (bin width). The probability in each bin is about 0.1, and the sum of all histogram area is 1 with 10 bins.

To confirm the results obtained with SFT, the plugin OrientationJ, Distribution in the ImageJ software was used (35) on the images previously assembled (with the same crop and Gaussian blur). As in SFT, protoplasts were divided in several ROIs (one ROI = 8 pixels). The orientation of CMTs in each ROI was measured. For each technical replicate, all of the orientations were then distributed into six classes of angles, ranging from 0° to 90°, each class measuring 15°. Data were normalized and histograms were constructed, displaying the proportion of ROIs in each class of angles. Both of these methods (i.e., SFT and OrientationJ plugin) allow a very local analysis of each microtubule orientation.

Correlation between protoplast deformation and CMT orientation was obtained with the OrientationJ, Dominant direction plugin. This plugin measures the mean orientation of microtubule in each cell. The cell deformation was estimated by drawing an ellipse around each protoplast with the ImageJ software and calculating a ratio between the major and the minor axis of that ellipse. The scatterplot represents the average orientation of the microtubule for each protoplast according to their aspect-ratio after confinement.

Statistical Analysis. Statistical tests were conducted with R software. Statistical analysis of the results (sample size [n], P value, type of test) is presented in *Results*.

Data Availability. All study data are included in the article and supporting information.

ACKNOWLEDGMENTS. We thank the MBI, Singapore, for hosting A.C. and O.H. for 6 months, where the original experiments were performed. We also thank our colleagues for constructive discussions about this project and for critical reading of the manuscript. We thank Platim for help with imaging and Gianluca Grenci for the design of the microwell casts at MBI. This work was supported by European Research Council Grant 615739 "MechanoDevo" (to O.H.), Ministry of Education, Culture, Sports, Science and Technology KAKENHI Grant-in-Aid for Scientific Research on Innovative Areas "Plant-Structure Optimization Strategy" GrantJP18H05484) (to S.T.) and MBI seed grant support (to V.V. and T.E.S.).

1. J. Sachs, *Über die Anordnung der Zellen in jüngsten Pflanzentheilen* (1878), 46–104.
2. L. Errera, Sur une condition fondamentale d'e´ quilibre des cellules vivantes. *C. R. Hebd. Seances Acad. Sci.* **103**, 822–824 (1886).
3. L. Kny, Über den Einfluß von Zug und Druck auf die Richtung der Scheidewände in sich teilenden Pflanzenzellen. *Ber Dtsch. Bot Gesell.* **14**, 378–391 (1896).
4. A. Guérin, S. Gravelle, J. Dumais, Forces behind plant cell division. *Proc. Natl. Acad. Sci. U.S.A.* **113**, 8891–8893 (2016).
5. T. I. Baskin, Anisotropic expansion of the plant cell wall. *Annu. Rev. Cell Dev. Biol.* **21**, 203–222 (2005).
6. D. J. Cosgrove, Growth of the plant cell wall. *Nat. Rev. Mol. Cell Biol.* **6**, 850–861 (2005).

7. J. Chan, E. Coen, Interaction between autonomous and microtubule guidance systems controls cellulose synthase trajectories. *Curr. Biol.* **30**, 941–947.e2 (2020).
8. A. R. Paredez, C. R. Somerville, D. W. Ehrhardt, Visualization of cellulose synthase demonstrates functional association with microtubules. *Science* **312**, 1491–1495 (2006).
9. V. Mirabet *et al*., The self-organization of plant microtubules inside the cell volume yields their cortical localization, stable alignment, and sensitivity to external cues. *PLoS Comput. Biol.* **14**, e1006011 (2018).
10. M. Cosentino Lagomarsino *et al*., Microtubule organization in three-dimensional confined geometries: Evaluating the role of elasticity through a combined in vitro and modeling approach. *Biophys. J.* **92**, 1046–1057 (2007).
11. P. Durand-Smet, T. A. Spelman, E. M. Meyerowitz, H. Jönsson, Cytoskeletal organization in isolated plant cells under geometry control. *Proc. Natl. Acad. Sci. U.S.A.* **117**, 17399–17408 (2020).
12. C. Ambrose, J. F. Allard, E. N. Cytrynbaum, G. O. Wasteneys, A CLASP-modulated cell edge barrier mechanism drives cell-wide cortical microtubule organization in Arabidopsis. *Nat. Commun.* **2**, 430 (2011).
13. A. Burian *et al*., A correlative microscopy approach relates microtubule behaviour, local organ geometry, and cell growth at the Arabidopsis shoot apical meristem. *J. Exp. Bot.* **64**, 5753–5767 (2013).
14. J. J. Lindeboom *et al*., A mechanism for reorientation of cortical microtubule arrays driven by microtubule severing. *Science* **342**, 1245533 (2013).
15. O. Hamant *et al*., Developmental patterning by mechanical signals in Arabidopsis. *Science* **322**, 1650–1655 (2008).
16. B. Chakrabortty *et al*., A plausible microtubule-based mechanism for cell division orientation in plant embryogenesis. *Curr. Biol.* **28**, 3031–3043.e2 (2018).
17. P. Green, A. King, A mechanism for the origin of specifically oriented textures in development with special reference to Nitella wall texture. *Aust. J. Biol. Sci.* **19**, 421–438 (1966).
18. O. Hamant, D. Inoue, D. Bouchez, J. Dumais, E. Mjolsness, Are microtubules tension sensors? *Nat. Commun.* **10**, 2360 (2019).
19. X. Gao *et al*., Artificial microniche array with spatially structured biochemical cues. *Methods Mol. Biol.* **1771**, 55–66 (2018).
20. S. Tsugawa *et al*., Extracting subcellular fibrillar alignment with error estimation: Application to microtubules. *Biophys. J.* **110**, 1836–1844 (2016).
21. Q. Li *et al*., Extracellular matrix scaffolding guides lumen elongation by inducing anisotropic intercellular mechanical tension. *Nat. Cell Biol.* **18**, 311–318 (2016).
22. D. Inoue *et al*., Sensing surface mechanical deformation using active probes driven by motor proteins. *Nat. Commun.* **7**, 12557 (2016).
23. H. Yan *et al*., Microtubule self-organisation during seed germination in Arabidopsis. *BMC Biol.* **18**, 44 (2020).
24. A. T. Molines *et al*., Physical properties of the cytoplasm modulate the rates of microtubule growth and shrinkage. bioRxiv:10.1101/2020.10.27.352716 (10 November 2020).
25. Z. Hejnowicz, A. Rusin, T. Rusin, Tensile tissue stress affects the orientation of cortical microtubules in the epidermis of sunflower hypocotyl. *J. Plant Growth Regul.* **19**, 31–44 (2000).
26. S. Robinson, C. Kuhlemeier, Global compression reorients cortical microtubules in Arabidopsis hypocotyl epidermis and promotes growth. *Curr. Biol.* **28**, 1794–1802.e2 (2018).
27. A. D. Franck *et al*., Tension applied through the Dam1 complex promotes microtubule elongation providing a direct mechanism for length control in mitosis. *Nat. Cell Biol.* **9**, 832–837 (2007).
28. K. Celler *et al*., "Microtubules in plant cells: Strategies and methods for immunofluorescence, transmission electron microscopy, and live cell imaging" in *Cytoskeleton Methods and Protocols*, R. H. Gavin, Ed. (Springer New York, 2016), pp. 155–184.
29. P. Durand-Smet, T. A. Spelman, E. M. Meyerowitz, H. Jönsson, Cytoskeletal organization in isolated plant cells under geometry control. bioRxiv:10.1101/784595 (1 March 2020).
30. J. Derr, R. Bastien, É. Couturier, S. Douady, Fluttering of growing leaves as a way to reach flatness: Experimental evidence on *Persea americana*. *J. R. Soc. Interface* **15**, 20170595 (2018).
31. S. Takatani *et al*., Microtubule response to tensile stress is curbed by NEK6 to buffer growth variation in the Arabidopsis hypocotyl. *Curr. Biol.* **30**, 1491–1503.e2 (2020).
32. T. Li *et al*., Calcium signals are necessary to establish auxin transporter polarity in a plant stem cell niche. *Nat. Commun.* **10**, 726 (2019).
33. C. M. Rounds, E. Lubeck, P. K. Hepler, L. J. Winship, Propidium iodide competes with Ca(2+) to label pectin in pollen tubes and Arabidopsis root hairs. *Plant Physiol.* **157**, 175–187 (2011).
34. W. Herth, E. Schnepf, The fluorochrome, calcofluor white, binds oriented to structural polysaccharide fibrils. *Protoplasma* **105**, 129–133 (1980).
35. R. Rezakhaniha *et al*., Experimental investigation of collagen waviness and orientation in the arterial adventitia using confocal laser scanning microscopy. *Biomech. Model. Mechanobiol.* **11**, 461–473 (2012).